Low-Energy Photoionization*

E. M. Henry,† C. L. Bates, and Wm. J. Veigele‡
Kaman Sciences Corporation, Colorado Springs, Colorado 80907
(Received 14 June 1972)

Low-energy-photoionization cross sections for the elements hydrogen through plutonium were calculated using a nonrelativistic single-particle model. Initial-atom and final-ion wave functions were developed from the Hartree–Fock equations using Slater's free-electron exchange approximation. Core relaxation was included approximately by using experimental binding energies in the Schrödinger equation for the continuum electron. Subshell contributions and total-cross-section calculations for the noble gases are compared with Hartree–Fock values with complete exchange. Total cross sections are compared with experiments for low-, medium-, and high-atomic-number elements.

INTRODUCTION

Attenuation of photons by atoms has been a phenomenon of interest for approximately a century. At photon energies between 0.1 and 10 keV, photoionization is the dominant attenuation mechanism with practically negligible contributions from other processes. Experimental data in this energy range are sparse. Most of the experimental data were obtained for the noble gases because of the relative ease with which those gases can be handled in the laboratory and because they are in the free-atom state. In addition, experimental data have been obtained only at selective photon energies because of the availability of x-ray line sources.

Extrapolations and interpolations of the experimental results yield values for elements at energies for which experiments were not performed, but knowledge of photon attenuation in this energy range still relies mainly on theory. Various theories have been developed, but, to date, none has been used to calculate a comprehensive set of photoionization cross sections for all elements over the energy range 0.1–10 keV. This is primarily because the more complete theories involve large amounts of computer time, and the simpler theories allowing quick calculations use relatively unrealistic models. Current reviews and bibliographies of the work above 1 keV are given by Storm and Israel[1] and Hubbell[2]; and reviews of theory down to 0.1 keV are given by Fano and Cooper,[3] Kennedy and Manson,[4] and Amusia, Cherepkov, and Chernysheva.[5]

The work reported here[6] uses a fairly realistic model with improved computational techniques involving moderate computational effort to obtain reliable calculations of photoionization cross sections over a range of low energies for all elements.

Theories for calculating photoelectric cross sections vary considerably in complexity. Effects such as electron exchange, multielectron correlations, and coupling in the final electron states have recently been considered in detail for selected elements.[3–5,7] Such effects have considerable influence on atomic cross sections at energies below approximately 0.1 keV, and on selected subshell contributions for higher energies. The computational difficulties involved in including these effects in their entirety for all elements, however, forces the consideration of approximations for the effects or neglect of them where possible.

In this paper we describe a model incorporating such approximations and present calculations of total photoionization cross sections for all elements from hydrogen through plutonium in the energy range 0.1–10 keV. Calculations were extended to 0.01 keV for the noble gases to examine the influence of the approximations used by comparing our results with experiment and earlier calculations. Electron exchange was included in the approximate form developed by Slater,[8] and core relaxation was included approximately by using experimental electron-binding energies in the wave equation for the continuum electron. Relativistic, multiparticle, and coupling effects were neglected.

THEORY

The contribution to the total photoionization cross section by an electron in the nl subshell of an atom was computed from the dipole central-field expression[9]

$$\tau_{nl} = \tfrac{4}{3}\pi\alpha a_0^2 N_{nl} h\nu\left[\left(\frac{l}{2l+1}\right) R_{l-1}^2 + \left(\frac{l+1}{2l+1}\right) R_{l+1}^2\right] , \tag{1}$$

where α is the fine-structure constant, a_0 is the Bohr radius, N_{nl} is the subshell occupation number, $h\nu$ is the photon energy in rydbergs, and $R_{l\pm1}$ are the radial matrix elements for the transition of the electron from the bound state with orbital quantum number l to continuum states with $l' = l \pm 1$. The electronic states of the ionic core

were assumed unchanged from their initial states, and transitions to discrete final states were neglected.

The radial matrix elements were found from the dipole-length expression

$$R_{l\pm1} = \int_0^\infty P_{nl}(r) r P_{\epsilon,l\pm1}(r)\, dr \ , \tag{2}$$

where r is the electron radial position in Bohr units, ϵ is the continuum electron energy, and $P_{nl}(r)$ and $P_{\epsilon,l\pm1}(r)$ are the bound and continuum radial wave functions, respectively, of the photoelectron. These wave functions were determined by solving the radial Schrödinger equation with $E_n < 0$ and $\epsilon > 0$ for the same central potential, where E_n is the total energy of the electron in the nth level. The potential $V(r)$ in the radial Schrödinger equation

$$\left(\frac{d^2}{dr^2} + V(r) + E_n - \frac{l(l+1)}{r^2}\right) P(r) = 0 \ , \tag{3}$$

in which E_n is in rydbergs and r is in Bohr units, was obtained by summing the nuclear Coulomb potential, the net electronic Coulomb potential, and the Slater[8] free-electron exchange potential.

For low-energy-photoionization calculations, exchange must be included at least in this approximate fashion, because for the large orbital quantum numbers of the outer subshells the centrifugal term cancels more of the attractive net Coulomb potential making the attractive exchange term a greater portion of the net attractive potential. Values of $V(r)$ in this approximation are listed for most elements by Herman and Skillman.[10]

In Hartree–Fock (HF) calculations with complete electron exchange[4] the radial-length expression agrees better with experiment near threshold than does the velocity expression, and the velocity expression agrees better at higher energies than does the length expression. Furthermore, smoothing of the electron exchange potential, as in the Slater free-electron exchange approximation used in the present work, gives results that agree with the HF length (HF-L) calculation near threshold and with the HF velocity (HF-V) calculation at higher energies. It appears that this treatment of the exchange portion of the Hamiltonian retains the best features of the length and velocity formalisms and is reasonable for calculating photoionization cross sections over a wide range of photon energies for many elements.

Bound-state wave functions were calculated by the HF self-consistent field method[11] for solving Eq. (3) and were normalized to satisfy the expression

$$\int_0^\infty P_{nl}^2(r)\, dr = 1 \ . \tag{4}$$

Continuum radial wave functions were obtained by numerical integration of Eq. (3), initiated at $r = 0$ with the small-r starting functions given by Hartree,[11] and normalized in energy by the method of Bates and Seaton[12] to the asymptotic form[9]

$$P_{\epsilon l}(r) = \epsilon^{-1/4} \sin[\epsilon^{1/2} r - \tfrac{1}{2} l\pi + Z' \epsilon^{-1/2} \ln(2\epsilon^{1/2} r) + \delta_l] \ , \tag{5}$$

where Z' is the residual ionic-charge number and δ_l is a constant phase shift. This procedure, described in detail by Cooper,[13] does not require knowledge of the phase shift, but it must be performed at a radius where the slope of the argument of the sine function in Eq. (5) is approximately constant. The slope of the argument is $\epsilon^{1/2} + \epsilon^{-1/2} r^{-1}$, which approaches the constant $\epsilon^{1/2}$ as r becomes large. Because the ratio of the second term to the first term in the slope is energy dependent, the normalization constant must be calculated at a different radius for different ϵ to obtain the same accuracy in the cross section for that subshell over the photon energy range.

Though the same wave functions were used for the ionic core electrons in their initial and final states, the effect of core relaxation on the continuum electron was included approximately by using experimental binding energies in the Schrödinger equation for the continuum radial wave function. The experimental energies used in this study were primarily those tabulated by Bearden and Burr,[14] Moore,[15] and Siegbahn *et al.*[16] They were combined, where necessary, to subshell energies according to electron occupation numbers. Energies for the $5f$ electrons were taken from Ref. 10 and other energies were interpolated.

Figure 1 for the xenon $5s$ subshell shows the effect on the photoionization cross section of using the experimental binding energy in the Schrödinger equation for the continuum wave function. The Hartree–Slater (HS) results including approximate core relaxation (HS_{cr}) from the present work are shifted from the HS results toward the HF-L curve, given in Ref. 4.

NUMERICAL PROCEDURES

Computations were performed on a CDC 6400 digital computer. Integrals were evaluated by the Simpson's rule quadrature method, and differential equations were solved by Runga–Kutta numerical methods. The running time for the total program varied from approximately 4 sec per subshell per photon energy at low-Z elements to about 5.5 sec per subshell per photon energy for high-Z elements. The computing time for our complete set of photoionization calculations was approximately 17 h.

Radial Matrix Elements

The radial matrix elements given by Eq. (2) were computed by using the basic Herman–Skill-

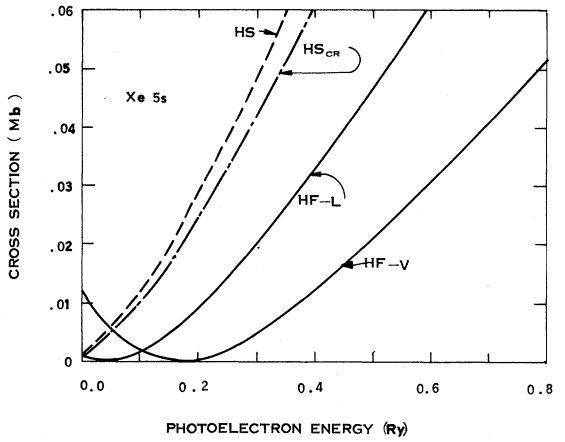

FIG. 1. Photoionization cross section of the 5s subshell of Xe; HF-L and HF-V are from Ref. 4; HS is from Ref. 4; HS_{cr} is the present calculation including approximate core relaxation.

man[10] integration intervals adjusted for each element and photoelectron energy. The intervals referred to here are $\frac{1}{4}$ the size of those published in Ref. 10. Adjustment of the interval size to ensure fairly constant integration accuracy over the range of elements and energies considered was accomplished by examining the oscillations of the continuum wave function. As the integration of Eq. (2) proceeded outward to larger interval sizes, the interval size was compared to $\frac{1}{20}$ the wavelength of the continuum wave function. If the interval size was greater, it was divided by 2 and compared again. When proper comparison was obtained, the bound-electron wave function was interpolated for values at the new integration points. Equation (3) for the continuum wave function was integrated in more refined steps by dividing the interval size used in Eq. (2) by 4 for $\epsilon \leq 50$ Ry and by 6 for $\epsilon > 50$ Ry.

Continuum Wave Function

The continuum wave function was determined from Eq. (3) by using the same central potential $V(r)$ that was used in determining the bound-electron wave function. The energy ϵ was found, however, by subtracting the experimental binding energy from the incident photon energy. Integration of Eq. (3) was started near $r = 0$ with the power-series expansion given by Hartree.[11] As the continuum wave function was evaluated step by step from Eq. (3) it was immediately substituted into Eq. (2) to eliminate the duplicate setup of the integration interval scheme.

Normalization of the continuum wave function is similar to that described in Appendix A of Ref. 13. By this technique, the normalization constant C can be determined without knowing the phase shift of the asymptotic form of the wave function. Here C is defined as the ratio of the asymptotic form to the unnormalized form of the wave function determined from Eq. (3). In eliminating the phase shift, it is proposed in Ref. 13 that determination of the slope $X \equiv d\theta/dr$ of the argument $\theta(r)$ of the asymptotic wave function

$$P_{\epsilon l} = \epsilon^{-1/4} \sin\theta(r) \ , \tag{6}$$

in which

$$\theta(r) \equiv \epsilon^{1/2} r - \tfrac{1}{2} l\pi + Z' \epsilon^{-1/2} \ln(2\epsilon^{1/2} r) + \delta_l \ , \tag{7}$$

be performed by examination of a second-order differential equation in X and r. We have determined the slope directly and examined it and the function $\theta(r)$ itself at two separate radii to eliminate the phase shift δ_l. In particular, since

$$X \equiv \frac{d\theta}{dr} = \epsilon^{1/2}\left(1 + \frac{1}{\epsilon r}\right) \ , \tag{8}$$

then, if

$$a_i \equiv X^{1/2}(r_i) P^n_{\epsilon l}(r_i) \tag{9}$$

and

$$\gamma \equiv \theta(r_2) - \theta(r_1) \ , \tag{10}$$

where $P^u_{\epsilon l}(r_i)$ is the unnormalized continuum wave function at radial distance r_i, and r_2 and r_1 are arbitrary but different values of r_i, it can be shown that the normalization constant is

$$C = \frac{\sin\gamma}{(a_1^2 + a_2^2 - 2a_1 a_2 \cos\gamma)^{1/2}} \ . \tag{11}$$

In regions where the denominator of Eq. (11) vanishes, C will be indeterminate, so the condition

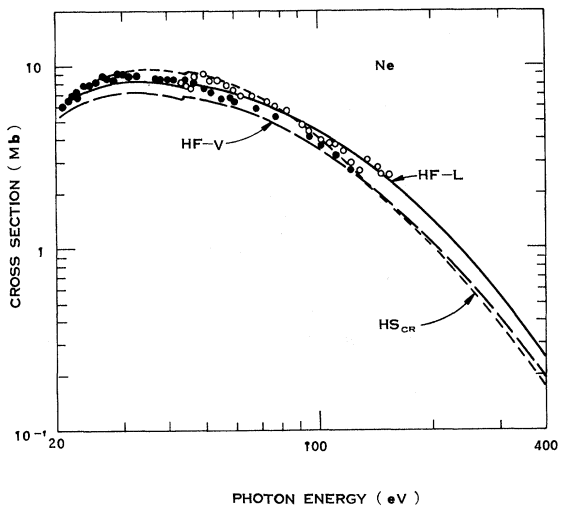

FIG. 2. Photoionization cross section for Ne. HS_{cr} is present work; HF-L and HF-V are from Ref. 4. Data points are closed circles from Ref. 17, open circles from Ref. 18.

$$a_1^2 + a_2^2 - 2a_1 a_2 \cos\gamma = 0 \qquad (12)$$

defines regions of numerical instability. Since $a_1 \simeq a_2$, indeterminacy may occur where $\gamma \simeq n\pi$, implying that

$$(a_1^2 + a_2^2)/2a_1 a_2 \simeq \pm 1 \ . \qquad (13)$$

Because $(1 - 1/\epsilon r_t)^{1/2} \simeq 1$ at either r_1 or r_2, Eq. (13) indicates numerical instability in C wherever the continuum wave function satisfies the condition

$$P(r_1) \simeq \pm P(r_2) \ . \qquad (14)$$

This condition may be satisfied when C is calculated near a positive or negative peak in the continuum wave function, or at a node.

The procedures used in calculating the normalization constant were designed, therefore, to meet the two criteria that (i) normalization was performed in the asymptotic region of the continuum wavefunction; and (ii) regions of calculational instability were avoided. Criterion (i) was satisfied by selecting $r_1 > r_0$, where r_0 was a radius greater than that for which the bound-electron wave function effectively vanished and for which the condition $1/\epsilon r_0 < 0.01$ was satisfied. This second condition assures that X is within 1% of the value $\epsilon^{1/2}$, and that the influence of the residual ion on the continuum electron is small. Criterion (ii) was satisfied by examining the slope of the wave function for a positive or negative peak, and then fixing r_1 a few intervals past the peak. Values of $r_2 > r_1$ were used to calculate C until two successive calculations showed a round-off agreement to four significant figures. Successive r_2 values were stepped off from the first r_2 by using $\frac{1}{5}$ the step size between r_1 and the first value of r_2. Selection of values for r_2 never proceeded past the point where the difference $r_2 - r_1$ equalled a quarter wavelength of the continuum wave function. Before C was calculated, the comparison $\sin^2\gamma \geq 0.001$ was made as an additional precaution against instability in the calculation.

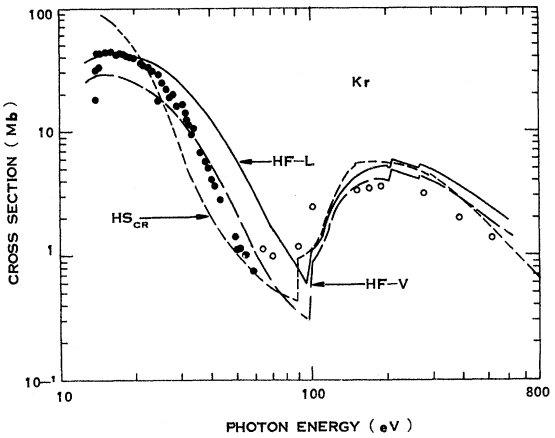

FIG. 4. Photoionization cross section for Kr. HS_{cr} is present work; HF-L and HF-V are from Ref. 4. Data points are closed circles from Ref. 17, open circles from Ref. 20.

RESULTS

Noble Gases

Figures 2–5 show our HS_{cr} results for neon, argon, krypton, and xenon compared with the HF-L and HF-V calculations from Ref. 4 and experimental values.[17–21] In Fig. 2 the agreement of the HS_{cr} results with the length calculation at low energies and the velocity calculation toward higher energies is evident. The same feature occurs for argon and krypton, and comparison with experi-

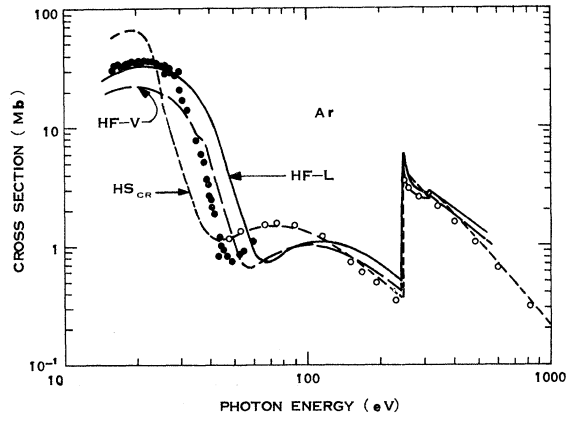

FIG. 3. Photoionization cross section for Ar. HS_{cr} is present work; HF-L and HF-V are from Ref. 4. Data points are closed circles from Ref. 17, open circles from Ref. 19.

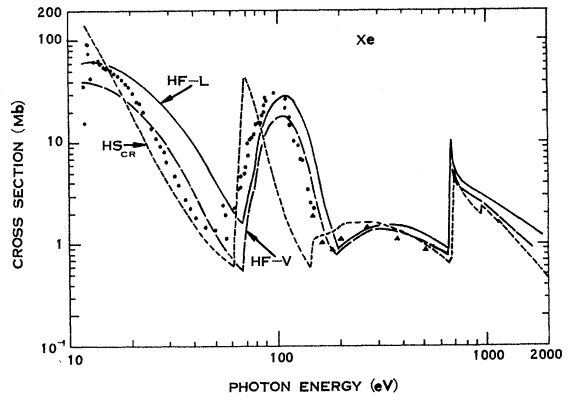

FIG. 5. Photoionization cross section for Xe. HS_{cr} is present work; HF-L and HF-V are from Ref. 4. Data points are closed circles from Ref. 17, open circles from Ref. 21, triangles from Ref. 20.

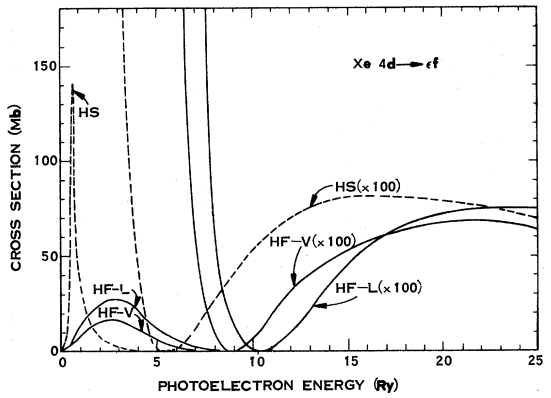

FIG. 6. Xe $4d \rightarrow \epsilon f$ partial photoionization cross section.

ments in Figs. 2–4 is good. The results for xenon in Fig. 5 begin to show the effect of the Slater exchange potential at low energies. In neon, argon, and krypton only p electrons contribute significantly to the cross section at 100–200-eV photon energies. In xenon, however, the $4d$ subshell is a major contributor and is primarily responsible for the Cooper minimum[3] observed near 200 eV.

The exchange effect is expected to be more significant for d electrons than for p electrons, and is responsible for the rather large discrepancy between the HS_{cr} and HF results between 150 and 200 eV in Fig. 5. This can be seen from comparison of the HS and HF results for the $4d$-subshell cross-section contribution in Xe, shown in Fig. 6 which is from Ref. 4. The HS cross section reaches a maximum approximately 30 eV closer to threshold than either of the HF results and drops off very rapidly at higher energies.

A similar comparison for the outer p electrons of Xe shown in Fig. 7, which also is from Ref. 4, shows much less discrepancy between the results with Slater exchange and those with complete exchange.

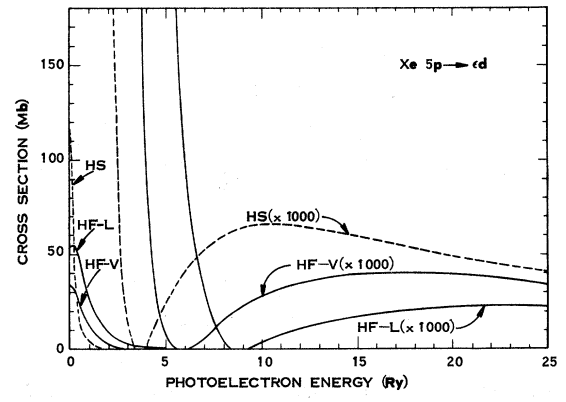

FIG. 7. Xe $5p \rightarrow \epsilon d$ partial photoionization cross section.

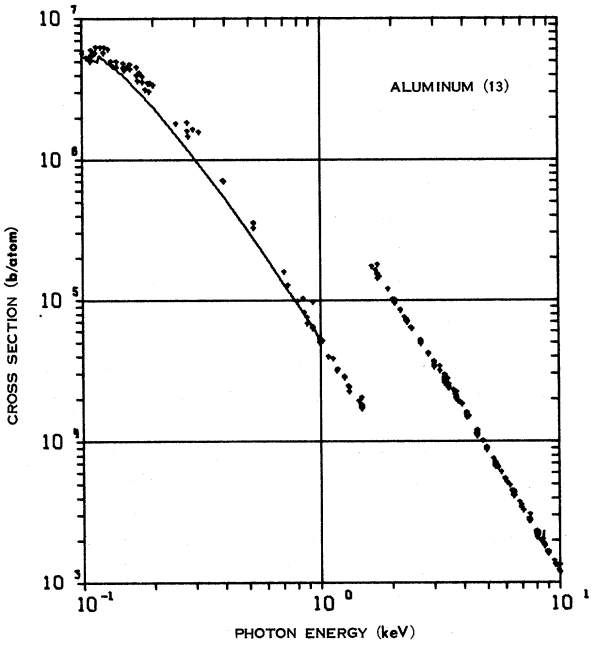

FIG. 8. Photoionization cross section for Al; data points are from Refs. 22–49.

Other Elements—Comparisons with Experiment

Calculations were made for photon energies from 0.1 keV to between 1.0 and 10 keV for all ele-

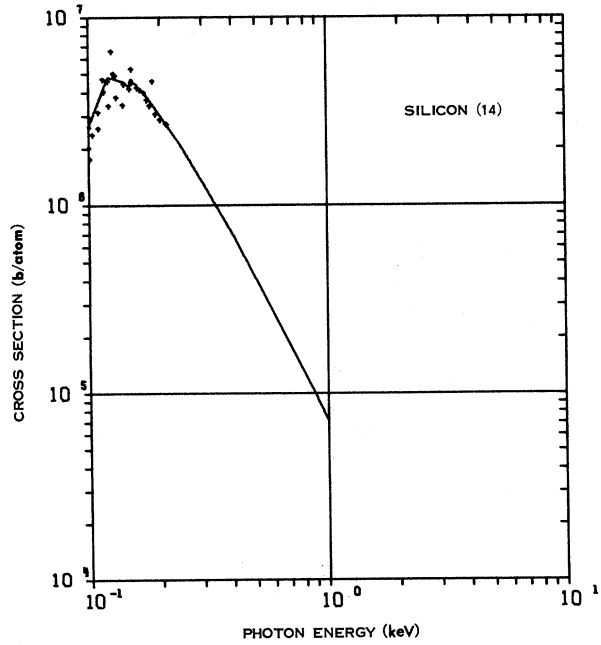

FIG. 9. Photoionization cross section for Si; data points are from Refs. 23, 50, and 51.

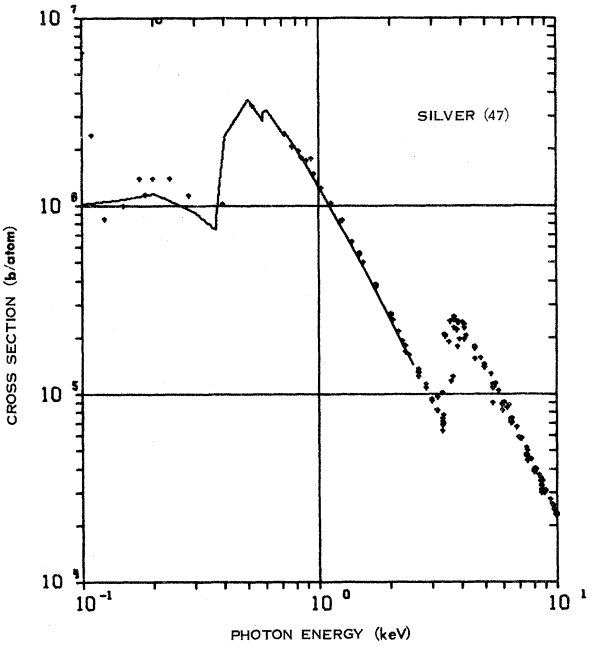

FIG. 10. Photoionization cross section for Ag; data points are from Refs. 26, 27, 34, 36, 39, 41–44, 48, 49, and 52–55.

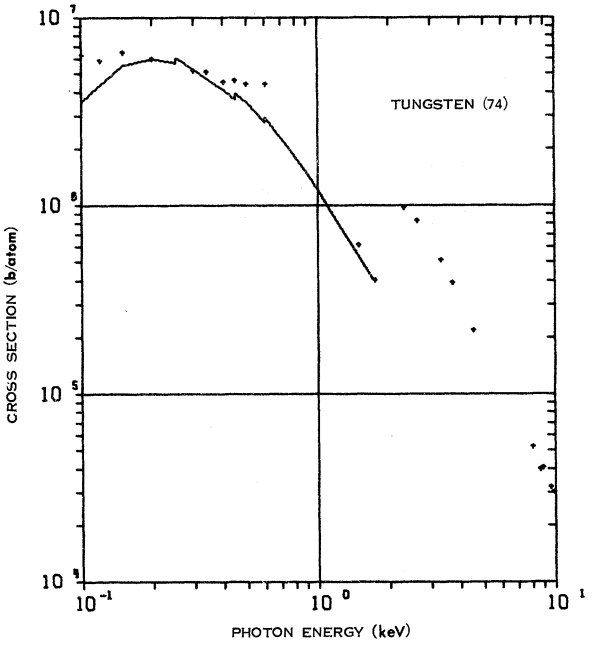

FIG. 12. Photoionization cross section for W; data points are from Refs. 22, 41, 49, and 60.

ments from hydrogen through plutonium, and graphical comparisons were made with experiment for 52 elements for which experimental data were available.[6] Sample comparisons with experiment are presented for aluminum, silicon, silver, tin, tungsten, and gold in Figs. 8–13. Comparison is

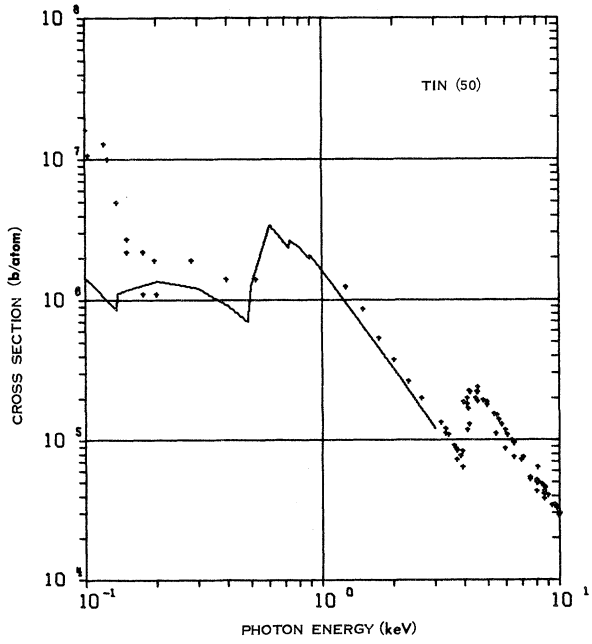

FIG. 11. Photoionization cross section for Sn; data points are from Refs. 27, 30, 39, 44, 45, 49, 52, and 55–59.

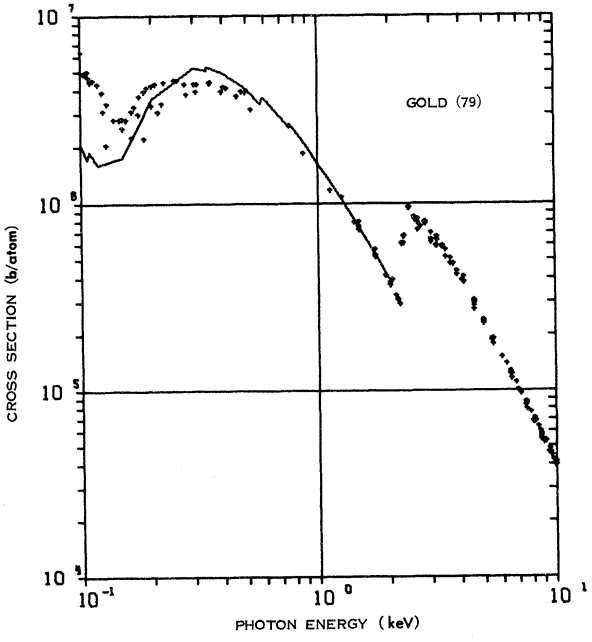

FIG. 13. Photoionization cross section for Au; data points are from Refs. 22, 26, 27, 30, 32, 36, 41, 42, 48, 49, 52, 54, 59, and 61–65.

good at all energies for low-Z elements and above approximately 0.2 keV for medium- and high-Z elements. The discrepancies below 0.2 keV in silver, tin, and gold are due to incomplete exchange in the d-subshell cross-section contributions, such as for xenon.

Though the discrepancy between theory and experiment has been shown here to be due mostly to the Slater exchange potential, multielectron correlations and the physical and chemical states of the experimental samples also affect the cross sections at low photon energies, especially near thresholds. Amusia, Cherepkov, and Chernysheva[5] have shown that though single-particle-model cross sections may vary from experimental values at threshold by as much as a factor of 2, theoretical cross sections that include multielectron correlations in addition to exchange are in good agreement with experiment. Jaegle *et al.*[61] also refer to effects from multiple-excitation mechanisms in the spectra of high-Z elements, and the possibility that part of the discrepancy between any free-atom theory and experiment is due to the crystalline structure of the absorbers.

CONCLUSIONS

The calculations agree qualitatively with experiments. Scatter in experimental data makes it difficult to assign quantitative uncertainties. For example, Kr and Xe between 10 and 20 eV and Si and Au between 0.1 and 0.2 keV in Figs. 4, 5, 9, and 13 show scatter varying from factors of 2–6, well beyond the experimental errors reported. Over many regions for which there are sufficient and consistent experimental data, uncertainties in our calculations are of an order of magnitude of 10%. Largest discrepancies appear at the lower energies for medium- to high-Z elements. Analysis of subshell cross-section contributions has shown the reason to be incomplete calculation of electron exchange and possibly lack of correlation.

ACKNOWLEDGMENTS

The authors are grateful to David Kennedy and Steve Manson for informative discussions and for allowing us to examine their computer program, and to Edith Briggs for assistance in preparing the manuscript.

---

*Work supported in part by the Defense Nuclear Agency.

†Permanent address: Air Force Technical Application Center, Patrick Air Force Base, Fla.

‡Also at the University of Colorado, Colorado Springs, Colo. 80907.

[1]E. Storm and H. I. Israel, Nucl. Data Tables 7, 565 (1970).

[2]J. H. Hubbell, Natl. Bur. Std. Report No. NSRDS-NBS 29, 1969 (unpublished).

[3]U. Fano and J. W. Cooper, Rev. Mod. Phys. 40, 441 (1968).

[4]D. J. Kennedy and S. T. Manson, Phys. Rev. A 5, 227 (1972).

[5]M. Ya Amusia, N. A. Cherepkov, and L. V. Chernysheva, Zh. Eksperim. i Teor. Fiz. 60, 160 (1971) [Sov. Phys. JETP 33, 90 (1971)].

[6]A preliminary account was given by Wm. J. Veigele, E. Briggs, L. Bates, E. M. Henry, and B. Bracewell, [Kaman Sciences Corp., Colorado Springs, Colo., Report No. DNA 2433F, 1971 (unpublished)]; Wm. J. Veigele, L. Bates, and E. M. Henry, Bull. Am. Phys. Soc. 16, 1354 (1971); E. M. Henry, L. Bates, and Wm. J. Veigele, *ibid.* 16, 1354 (1971).

[7]H. Kelly and A. Ron, Phys. Rev. Letters 26, 1359 (1971).

[8]J. C. Slater, Phys. Rev. 81, 385 (1961).

[9]H. A. Bethe and E. E. Salpeter, *Quantum Mechanics of One- and Two-Electron Atoms* (Springer-Verlag, Berlin, 1957), p. 295.

[10]F. Herman and S. Skillman, *Atomic Structure Calculations* (Prentice-Hall, Englewood Cliffs, N. J., 1963).

[11]D. R. Hartree, *The Calculation of Atomic Structures* (Wiley, New York, 1957), p. 81.

[12]D. R. Bates and M. F. Seaton, Monthly Notices Roy. Astron. Soc. 109, 698 (1949).

[13]J. W. Cooper, Phys. Rev. 128, 681 (1962).

[14]J. A. Bearden and A. F. Burr, Rev. Mod. Phys. 39, 125 (1967).

[15]C. E. Moore, Natl. Bur. Std. Report No. NSRDS-NBS 34, 1970 (unpublished).

[16]K. Siegbahn *et al.*, *ESCA, Atomic, Molecular and Solid State Structure Studies by Means of Electron Spectroscopy* (Almgvist & Wicksells Boktryckeri AB, Uppsala, 1967).

[17]J. A. R. Sampson, in *Advances in Atomic and Molecular Physics*, edited by D. R. Bates and I. Esterman (Academic, New York, 1966), Vol. II, p. 178.

[18]D. L. Ederer and D. H. Tomboulian, Phys. Rev. 133, A1525 (1964).

[19]A. P. Lukirskii and T. M. Zimkina, Bull. Acad. Sci. USSR 27, 808 (1963).

[20]A. P. Lukirskii, I. A. Brytov, and T. M. Zimkina, Opt. i Spectroskopiya 17, 438 (1964) [Opt. Spectry. 17, 234 (1964)].

[21]D. L. Ederer, Phys. Rev. Letters 13, 760 (1964).

[22]P. Lublin, P. Cukor, and R. J. Jaworowski, *Advances in X-Ray Analysis* (Plenum, London, 1970), p. 632.

[23]C. Gahwiller and F. C. Brown, Phys. Rev. B 2, 1918 (1970).

[24]R. Haensel *et al.*, J. Appl. Phys. 40, 3046 (1969).

[25]P. M. Raccah and V. E. Henrich, Phys. Rev. 184, 607 (1969).

[26]G. D. Hughes *et al.*, Brit. J. Appl. Phys. 1, 695 (1968).

[27]P. K. Hon and K. F. J. Heinrich (private communication). NBS experimental data.

[28]S. Singer, J. Appl. Phys. 38, 2897 (1967).

[29]V. A. Fomichev and A. P. Lukirskii, Opt. i Spectroskopiya 22, 796 (1967) [Opt. Spectry. 22, 432 (1967)].

[30]A. J. Bearden, J. Appl. Phys. 37, 1681 (1966).

[31]K. F. J. Heinrich, in *The Electron Microprobe*,

edited by T. D. McKinley (Wiley, New York, 1966), p. 296.
[32]J. B. Woodhouse (private communication). Metals Research data (1966).
[33]M. J. Cooper, Acta Cryst. 18, 813 (1965).
[34]B. A. Cooke and E. A. Stewardson, Brit. J. Appl. Phys. 15, 1315 (1964).
[35]W. T. Ogier *et al.*, Appl. Phys. Letters 5, 146 (1964).
[36]A. P. Lukirskii *et al.*, Opt. i Spectroskopiya 16, 310 (1964) [Opt. Spectry. 16, 168 (1964)].
[37]B. A. Cooke *et al.*, Proc. Phys. Soc. (London) 79, 883 (1962).
[38]P. R. Wise, M. A. thesis (Johns Hopkins University, 1961) (unpublished).
[39]C. E. Ehrenfried and D. E. Dodds, Kirtland Air Force Base Report No. AFSWC TN 59-33, 1960 (unpublished).
[40]J. I. Hopkins, J. Appl. Phys. 30, 185 (1959).
[41]R. D. Deslattes, Department of Physics, Florida State University, Report No. AFOSR TN 58-784, 1958 (unpublished).
[42]C. L. Andrews, Phys. Rev. 54, 994 (1938).
[43]R. D. Hill, Proc. Roy. Soc. (London) A161, 284 (1937).
[44]H. H. Biermann, Ann. Physik 26, 740 (1936).
[45]K. Grosskurth, Ann. Physik 20, 197 (1934).
[46]J. A. Crowther and L. H. H. Orton, Phil. Mag. 13, 505 (1932).
[47]W. W. Colvert, Phys. Rev. 36, 1619 (1930).
[48]I. Backhurst, Phil. Mag. 7, 353 (1929).
[49]S. J. M. Allen, Phys. Rev. 28, 907 (1926).
[50]O. A. Ershov and A. P. Lukirskii, Fiz. Tverd. Tela 8, 2137 (1966) [Sov. Phys. Solid State 8, 1699 (1967)].
[51]D. H. Tomboulian and D. E. Bedo, Phys. Rev. 104, 590 (1956).
[52]R. Haensel *et al.*, Phys. Letters 25, 205 (1967).
[53]B. Nordfors, Arkiv Fysik 19, 259 (1961).
[54]K. Schulz, Ann. Phys. (Paris) 27, 1 (1936).
[55]L. N. Martin and K. C. Lang, Proc. Roy. Soc. (London) A137, 199 (1932).
[56]K. Codling *et al.*, J. Opt. Soc. Am. 56, 189 (1966).
[57]A. P. Lukirskii *et al.*, Fiz. Tverd. Tela 8, 1929 (1966) [Sov. Phys. Solid State 8, 1525 (1966)].
[58]B. Nordfors and E. Noreland, Arkiv Fysik 20, 1 (1961).
[59]S. Laubert, Ann. Physik 40, 553 (1941).
[60]R. Haensel *et al.*, Solid State Commun. 7, 1495 (1969).
[61]P. Jaegle, F. Combet Farnoux, P. Dhez, M. Cremonese, and G. Onori, Phys. Rev. 188, 30 (1969).
[62]O. A. Ershov, Opt. i Spectroskopiya 22, 468 (1967) [Opt. Spectry. 22, 252 (1967)].
[63]P. Jaegle and G. Missoni, C. R. Acad. Sci. (Paris) B262, 71 (1966).
[64]P. Matin, M. S. thesis (Vanderbilt University, 1960) (unpublished).
[65]E. Dershem and M. Schein, Phys. Rev. 37, 1238 (1931).

PHYSICAL REVIEW A VOLUME 6, NUMBER 6 DECEMBER 1972

Microscopic Optical-Model Analysis of Electron Scattering from Atomic Hydrogen*

G. D. Alton, W. R. Garrett, M. Reeves, and J. E. Turner
Oak Ridge National Laboratory, Oak Ridge, Tennessee 37830
(Received 13 July 1972)

The projection-operator formalism advanced by Feshbach is used to derive a numerically tractable equation which describes the elastic scattering of electrons from atomic hydrogen under multichannel conditions. By neglecting the potential of interaction in the inverse operator, analytical expressions can be obtained for the Green's function which permit the inclusion of both discrete and continuum target-state contributions to the optical potential. The numerical procedures used to solve the resulting nonlocal integrodifferential equation and to generate differential, total elastic and inelastic cross sections are discussed. Good agreement is found with available experimental data.

I. INTRODUCTION

The theoretical determination of atomic and molecular scattering cross sections in the low-energy region is greatly complicated by the presence of a large (usually infinite) number of open scattering channels. Thus, in order to obtain an accurate description of scattering phenomena for charged particles of energy below the region where the Born approximation is valid, effects due to the various inelastic processes which may occur must be included. The usual practice of expanding the total wave functions in terms of a set of target eigenfunctions leads to an infinite set of coupled differential equations which describe the scattering probabilities for elastic and inelastic processes. The difficulties associated with large coupled sets of equations preclude accurate solutions for all but a very limited range of projectile energies.[1]

Two important effects that should be accounted for at low energies in electron scattering from atoms and molecules are exchange and polarization. Exchange arises as a result of the Pauli principle